

Characterization of Ion-Beam-Sputtered AlF_3 Thin Films for Gravitational-Wave Interferometers

M. Bischì,^{1,2,*} A. Amato^④,⁴ M. Bazzan^④,⁶ G. Cagnoli,⁴ M. Canepa,^{7,8} G. Favaro^④,⁶ D. Forest^④,³
 P. Gobbi,⁵ M. Granata^④,^{3,†} G.M. Guidi,^{1,2} G. Maggioni^④,⁶ F. Martelli^④,^{1,2} M. Menotta^④,⁵
 M. Montani,^{1,2} F. Piergiovanni,^{1,2} and L. Valentini⁵

¹Dipartimento di scienze pure e applicate, Università degli Studi di Urbino “Carlo Bo”, Urbino I-61029, Italy

²INFN, Sezione di Firenze, Sesto Fiorentino, Firenze I-50019, Italy

³Laboratoire des Matériaux Avancés - IP2I, CNRS, Université de Lyon, Université Claude Bernard Lyon 1, Villeurbanne F-69622, France


⁴Université de Lyon, Université Claude Bernard Lyon 1, CNRS, Institut Lumière Matière, Villeurbanne F-69622, France

⁵Dipartimento di scienze biomolecolari, Università degli Studi di Urbino “Carlo Bo”, Urbino I-61029, Italy

⁶Università di Padova, Padova I-35131, Italy

⁷OPTMATLAB, Dipartimento di Fisica, Università di Genova, Via Dodecaneso 33 Genova 16146, Italy

⁸INFN, Sezione di Genova, Via Dodecaneso 33, Genova 16146, Italy

 (Received 24 February 2022; revised 4 June 2022; accepted 6 September 2022; published 22 November 2022)

Thermal noise in amorphous coatings is a limitation for a wide range of precision experiments such as gravitational-wave detectors (GWDs). Mirrors for GWDs are composed of multiple thin layers of dielectric materials deposited on a substrate: the stack is made of layers with a high-refractive index interleaved with layers of a low-refractive index. The goal is to obtain high reflectivity and low thermal noise. In this paper we report on the optical and mechanical properties of ion-beam-sputtered aluminium fluoride (AlF_3) thin films that have one of the lowest refractive indexes among the known coating materials and we discuss their application in current and future GWDs.

DOI: [10.1103/PhysRevApplied.18.054074](https://doi.org/10.1103/PhysRevApplied.18.054074)

I. INTRODUCTION

Brownian thermal noise in coatings (hereafter coating thermal noise, CTN) is a limiting noise source for precision experiments based on optical and quantum transducers. For example, the sensitivity of interferometric gravitational-wave detectors (GWDs) is limited in the frequency range around 100 Hz by CTN [1–3]. GWDs are Michelson interferometers with mirrors placed at the ends of two Fabry-Pérot cavities, in order to measure the relative motion of the two arms.

Mirrors for GWDs are Bragg reflectors composed of a stack of thin layers of two alternated dielectric materials (with high- and low-refractive index) deposited on a substrate. It is crucial to find coatings with low optical loss (absorption, scatter) and low thermal noise in order to improve the sensitivity of GWDs.

The power spectral density of thermally induced surface fluctuations is determined by the rate of energy dissipation

in each coating material, as stated by the fluctuation-dissipation theorem [4]: the higher the energy loss, the higher the CTN.

As measured with a laser beam, the CTN power spectral density S_{CTN} can be written as [5]

$$S_{\text{CTN}} \propto \frac{k_B T}{2\pi f} \frac{t_c}{w^2} \varphi_c(f, T), \quad (1)$$

where k_B is the Boltzmann constant, f is the frequency, T is the temperature, t_c is the coating thickness, w is the laser beam radius (where intensity drops by $1/e^2$), and $\varphi_c(f, T)$ is the loss angle associated with energy dissipation in the coating in the whole Bragg reflector, for GWDs [5,6] and corresponds to its internal mechanical friction.

Thus, S_{CTN} can be reduced by increasing the beam radius w , decreasing the temperature T , or by choosing coating materials that minimize $t_c \varphi_c$; furthermore, the lowest CTN is expected to occur when the Young modulus of the coating (Y_c) matches the elastic modulus of the substrate [5].

The reflectivity of a Bragg mirror depends on the number of low- and high-index layer pairs and on the refractive-index contrast $c = n_H/n_L$, where n_H and n_L are

*m.bischi1@campus.uniurb.it

†m.granata@lma.in2p3.fr

the high- and low-refractive indices, respectively. Using materials with higher c allows us to use a lower number of layers and, hence, a lower thickness of the entire stack t_c .

Up to now, the high-reflectivity (HR) coatings of the Advanced LIGO [7], Advanced Virgo [8] and KAGRA [9] GWDs are thickness-optimized stacks [10] of layers of tantalum pentoxide (Ta_2O_5) doped with a relevant fraction of titanium dioxide (TiO_2), also known as *titania-doped tantala* that is a high-index material and silicon dioxide (SiO_2), *silica*, a low-index material [6]. These HR coatings are deposited by the Laboratoire des Matériaux Avancés (LMA) [11,12] using the ion-beam sputtering (IBS) technique. Despite the excellent mechanical and optical properties of the current HR coatings [6,11], CTN remains a severe limitation for further sensitivity enhancements in GWDs. In the last two decades, a lot of effort has been committed to find an alternative high-index material [13,14], that is the most dissipative one at room temperature, but for present and future cryogenic GWDs like KAGRA [9], Einstein Telescope [15], and Cosmic Explorer [16], there is a need to find alternative low-CTN materials: in fact, the currently available data on IBS silica shows a dramatic increase of dissipation below 30 K [17,18], so a silica coating should be replaced by another low-refractive-index material featuring low mechanical and optical losses. Because of their low-refractive index [19–22] and potentially low mechanical loss at low temperature [23], fluoride coatings could be a valid option for use in cryogenic GWDs. So far, however, fluoride coatings have never been considered for implementation in gravitational-wave detectors such that a specifically oriented characterization of their properties is needed. The aim of this paper is to provide optical and mechanical properties of IBS aluminium fluoride (AlF_3) coatings as replacement of the low-index silica layers in the HR coatings of current and future GWDs. As a first step, we report the (AlF_3) properties measured at ambient temperature and we compare them with those of low-index silica films.

We take special care to characterize the impact of post-deposition thermal treatment on coating properties, in particular on φ_c . Such treatment (*annealing* hereafter) is a standard procedure for the production of the HR coatings of GWDs, as it usually allows us to improve their adhesion to the substrate as well as their optical qualities, and decrease their loss angle φ_c [6]. Annealing is performed inside a tube furnace in an argon-saturated atmosphere, in order to avoid surface oxidation.

II. METHODS

A. Samples

A thin layer of AlF_3 is deposited by IBS at the Laser Zentrum Hannover [24] on both sides of fused silica substrates (diameter 50 mm, $t = 1$ mm) for mechanical

TABLE I. Measured properties of silica disks for the characterization of mechanical losses.

	Sample A	Sample B
Diameter (mm)	49.94 ± 0.02	49.79 ± 0.02
Thickness (mm)	1.0 ± 0.1	1.0 ± 0.1
Mass before coating (mg)	4647.3 ± 0.1	4612.3 ± 0.1
Mass after coating (mg)	4649.1 ± 0.1	4613.9 ± 0.1
Coating thickness on each side (nm)	211 ± 6	211 ± 6

characterization and on one side of the silicon substrates (diameter 75 mm) for ion-beam analysis, x-ray diffraction measurements, and optical characterization. The coating is deposited on both sides of the fused silica substrates in order to have balanced stresses and avoid deformations of the disk that could produce a variation in resonant frequencies and affect the evaluation of the frequency-dependent dilution factor.

Prior to deposition, fused-silica disks are annealed in air at 900°C for 10 h to release the internal stress due to manufacturing. Their masses and mechanical losses are measured so that the coating losses can be calculated as explained in Sec. II D.

Prior to deposition, the base pressure inside the coater vacuum chamber is 5×10^{-6} mbar. The total pressure during the coating process is of the order of 10^{-4} mbar, with noble gases and gases containing fluorine injected into the chamber. The energy and current of the sputtering ions are of the order of 1 keV and 0.1 A, respectively.

B. Structure and chemical composition

In order to determine the chemical composition of the coating samples after deposition, as well as its change after annealing treatments, we perform a series of RBS measurements. These measurements are done in the Accelerator AN2000 at the INFN-LNL using a $^4\text{He}^+$ ion beam at 2 MeV in normal incidence, with a scattering angle of 160° .

Moreover, a series of grazing-incidence x-ray diffraction (GIXRD) measurements are performed on coating samples after the deposition and after different annealing steps, in order to determine the coating microscopic structure and its evolution with thermal treatments. GIXRD measurements are done with a Philips MRD diffractometer that is equipped with a Cu tube operated at 40 kV and 40 mA (collimated and partially monochromatized to the Cu K- α_1 line using a parabolic multilayer mirror) and with a detector provided with a parallel-plate collimator.

C. Optical properties

We use two J. A. Woollam spectroscopic ellipsometers to measure the coating optical properties, covering complementary spectral regions from ultraviolet to infrared: a VASE for the 0.73–6.53 eV photon energy range (corresponding to a 190–1700-nm wavelength range) and a M-2000 for the 0.74–5.06 eV range (245–1680 nm). The coated wafers are measured in reflection, their complex reflectance ratio is characterized by measuring its amplitude component Ψ and phase difference Δ [25]. To maximize the response of the instruments, the (Ψ, Δ) spectra are acquired at different incidence angles ($\theta = 50^\circ, 55^\circ, 60^\circ$) close to the coating Brewster angle. Coating refractive index and thickness are derived by fitting the spectra with realistic optical models [25]. The optical response of the bare wafers is characterized with prior dedicated measurements. Further details about our ellipsometric analysis are available elsewhere [26].

We use photothermal deflection [27] to measure the coating optical absorption at $\lambda = 1064$ nm with an accuracy of less than 1 part per million (ppm).

D. Mechanical properties

Two silica disks (A and B) are used for the characterization of the coating mechanical properties.

Before and after each treatment (coating deposition, annealing runs) we measure the mass of the disks with an analytical balance and we observe the surface with an optical microscope (Olympus IX51 equipped with a Toupcam camera) to check if the coating surface is deteriorated by each treatment. The properties of the silica disks are summarized in Table I.

We use the ringdown method [28] to measure the frequency f and ringdown time τ of several vibrational modes of each disk, before and after the coating deposition (and after each annealing treatment) in order to calculate the coating loss angle

$$\varphi_c = \frac{\varphi + (D - 1)\varphi_0}{D}, \quad (2)$$

where $\varphi = (\pi f \tau)^{-1}$ is the measured loss angle of the coated disk, $\varphi_0 = (\pi f_0 \tau_0)^{-1}$ is the measured loss angle of

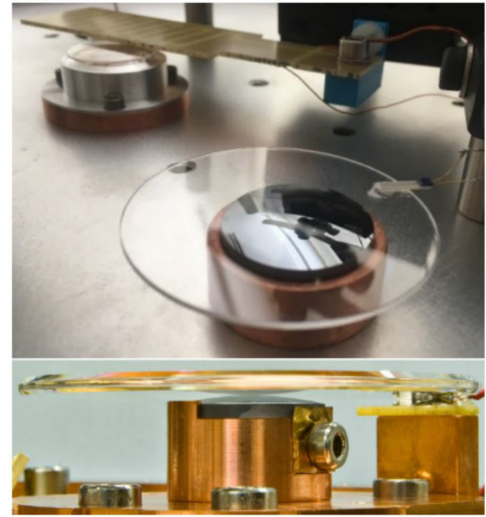


FIG. 1. GeNS systems used at the University of Urbino (top) and at LMA (bottom) to perform internal friction measurements. The sample is suspended in equilibrium on a sapphire or silicon hemisphere touching on one of the nodal points of vibration.

the bare substrate, D is the frequency-dependent measured dilution factor [29]

$$D = 1 - \left(\frac{f_0}{f}\right)^2 \frac{m_0}{m}, \quad (3)$$

where m_0 and m are the disk masses as measured before and after the coating deposition, respectively.

In order to minimize coating mechanical loss φ_c and optical absorption α , we test different plateau temperatures T_a and duration Δt_a . During the annealing, samples are held in a quartz box inside the oven and maintained in a controlled argon atmosphere during the entire process. Inbetween measurements, the samples are stored under primary vacuum (10^{-2} – 10^{-1} mbar) to avoid oxidation from air exposure.

Disks are first measured at the LMA before and after coating deposition, then measured, annealed, and measured again at Università degli Studi di Urbino Carlo Bo (UniUrb). Since the temperature in the two laboratories is different, a correction of measured mode frequencies

TABLE II. Relative atomic concentrations (%), Al:F atomic ratio and density ρ of IBS AlF₃ coatings before and after thermal treatments, obtained from SRIM database for stopping powers [34] of the RBS spectrum. The density is calculated by assuming a layer thickness of 211 nm for all samples (measured on as-deposited samples using a spectroscopic ellipsometry).

	Al	F	O	Xe	Mo	Cu	Ta	Al:F	ρ (g/cm ³)
As deposited	25.7	65	8	0.78	0.42	0.05	0.039	0.40	2.7
200 °C	27.5	63	8	0.82	0.49	0.11	0.041	0.43	2.8
300 °C	28.8	58	12	0.7	0.44	0.06	0.038	0.50	2.7
400 °C	29.8	60	9	0.6	0.42	0.12	0.036	0.50	2.3
500 °C	33.5	45	20	0.95	0.46	0.08	0.039	0.72	1.8

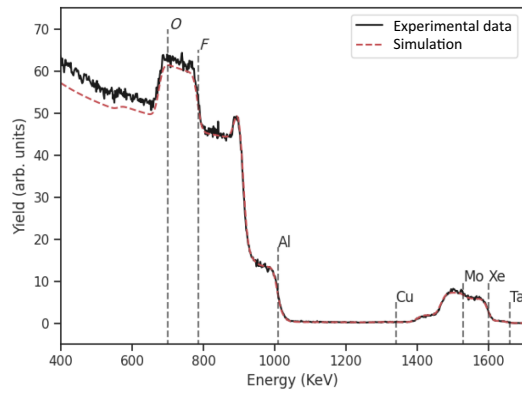


FIG. 2. Example of an RBS measurement (black line) and best fit (red line) obtained with SRIM database for stopping powers [34]. This graph is referred to as the as-deposited IBS AlF_3 coating.

is necessary for a correct evaluation of the frequency-dependent dilution factor, as explained in Ref. [30].

We measure resonant modes from approximately 2.5 kHz to approximately 50 kHz for each sample, in a frequency band that partially overlaps with the detection band of ground-based GWDs ($10\text{--}10^4$ Hz). For these ringdown measurements, we use two clamp-free in-vacuum gentle nodal suspension (GeNS) systems [31]. This kind of facility is currently the preferred solution of the Virgo and LIGO collaborations for performing internal friction measurements because it avoids systematic damping from suspension, clamp, or residual gas pressure [6,32].

The coating Young modulus Y_c and Poisson ratio ν_c are estimated by fitting finite-element simulations to measured dilution factors via least-squares numerical regression [6]. Further details about our GeNS systems, finite-element simulations, and data analysis are available elsewhere [6,33].

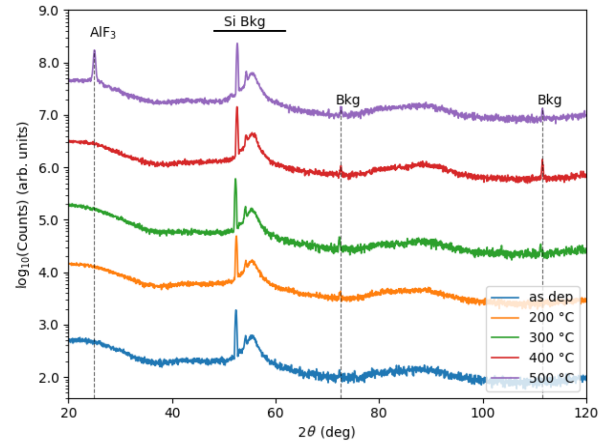


FIG. 3. GIXRD diffractograms of IBS AlF_3 coatings on silicon substrates, acquired before and after annealing treatments at different temperatures. Peaks between 50° and 60° are due to the background signal of the silicon substrate. The sample treated at 500°C shows an additional peak at $2\theta = 25^\circ$, compatible with the AlF_3 crystalline spectrum [35]. Peaks at $2\theta = 70^\circ$ and 110° are likely due to the background signal too; see the main text for more details.

III. RESULTS

A. Structure and chemical composition

RBS results of the coating samples are listed in Table II. Relative atomic concentrations and density ρ are deduced from simulations of the experimental spectra based on stopping powers drawn from the SRIM database [34]. Figure 2 shows an example of a RBS measurement, referred to as the as-deposited IBS AlF_3 coating. RBS analysis of the as-deposited film shows that the Al:F atomic ratio is slightly higher than the stoichiometric one (0.4 instead of 0.33): the missing F is partially compensated by O incorporation (8%). Moreover, the sample is contaminated by the Xe sputtering gas and by Mo from the sputtering source grids and contains traces of Cu and Ta.

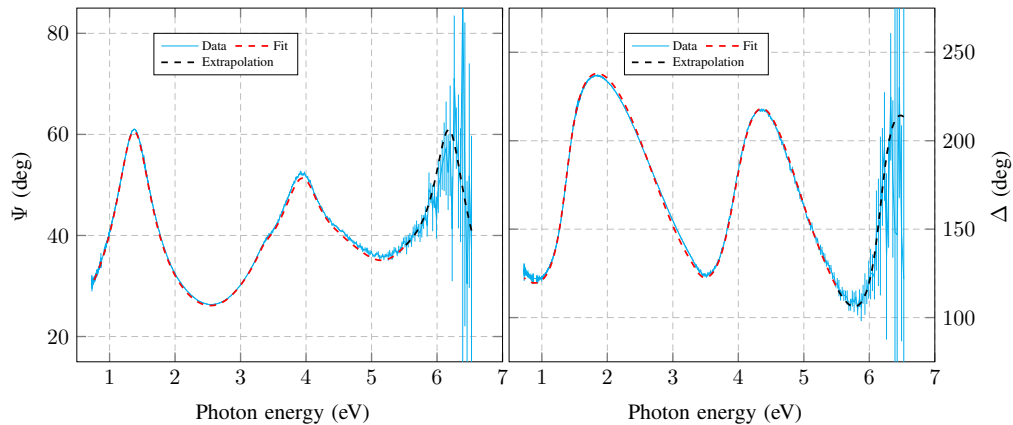


FIG. 4. Measured ellipsometric spectra of as-deposited IBS AlF_3 thin films, acquired at an incidence angle $\theta = 60^\circ$.

TABLE III. Refractive index n , extinction coefficient k , and density ρ of as-deposited IBS AlF_3 thin films. The n and k values presented in this work are measured in the 190–1700-nm wavelength range via spectroscopic ellipsometry. The k value at 1064 nm is deduced from photothermal deflection measurements of optical absorption, by assuming negligible scatter loss. (*)Extrapolations.

		This work	Kolbe <i>et al.</i> [20]	Yoshida <i>et al.</i> [21]	Ode [22]
n	1550 nm	1.356 ± 0.005			
k		$< 10^{-3}$			
n	1064 nm	1.358 ± 0.005			
k		$(5.06 \pm 0.01) \times 10^{-5}$			
n	633 nm	1.362 ± 0.005			
k		$< 10^{-3}$			
n	193 nm	1.4 (*)	1.41	1.43	1.42
k		1.4×10^{-2} (*)	5×10^{-4}	1.3×10^{-4}	8.3×10^{-6}
ρ (g/cm^3)		2.2 ± 0.4			

Film density is calculated by dividing the areal atomic density (obtained from RBS) by the layer thickness measured via spectroscopic ellipsometry, to find a value of $\rho = 2.7 \text{ g}/\text{cm}^3$.

RBS analysis of the annealed samples highlights the effect of annealing treatments on the film composition. The increase of the Al:F atomic ratio, which is small at the lower temperatures, becomes particularly pronounced in the sample annealed at 500°C and is accompanied by a release of fluorine (approximately 40%) and by an increase of the incorporated oxygen (+100%). Film density is also affected by the annealing treatments and decreases to $1.8 \text{ g}/\text{cm}^3$ in the sample annealed at 500°C . Concerning the other elements present in the film, annealing treatments do not seem to influence their atomic concentration, even at the highest temperature.

The GIXRD diffractograms of the coating samples are reported in Fig. 3. Peaks between 50° and 60° are due to the

background signal of the crystalline silicon substrate and are visible in all the spectra. The coating material remains amorphous with the exception of the sample treated at 500°C that displays a peak at $2\theta = 25^\circ$, compatible with AlF_3 crystalline spectrum that has a main peak at 25.3° [35]. The absence of other peaks is probably due to the fact that other peaks of AlF_3 are much less intense. There are some peaks around 70° and 110° whose origin is not known. Their presence seems not to be related to annealing treatments and they are not compatible with the AlF_3 crystalline spectrum, so they are probably associated to a background signal (likely due to contamination on the sample holder).

B. Optical properties

Figure 4 shows exemplary (Ψ, Δ) spectra of the as-deposited coatings, acquired at an incidence angle $\theta = 60^\circ$. At higher energy, above 5.7 eV, sample

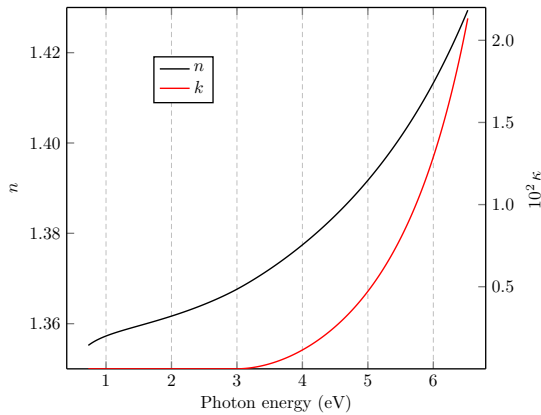


FIG. 5. Refractive index n and extinction coefficient k of as-deposited IBS AlF_3 thin films as a function of photon energy, derived from ellipsometric measurements. Relevant values for present and future GWDs are 0.80 and 1.17 eV, corresponding to a laser wavelength of 1550 and 1064 nm, respectively. For energy values smaller than approximately 3.5 eV, the extinction is smaller than the sensitivity of the ellipsometers ($k < 10^{-3}$).

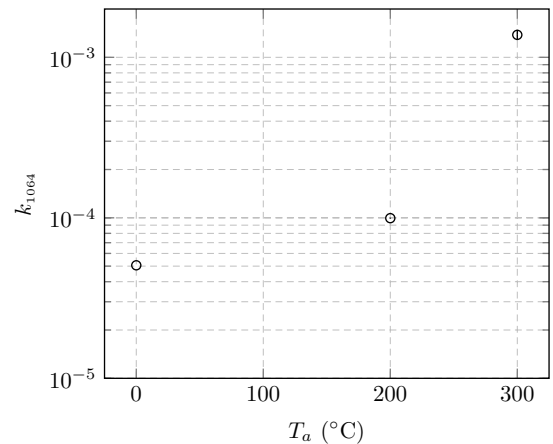


FIG. 6. Extinction coefficient k_{1064} of IBS AlF_3 thin films as a function of the annealing temperature T_a , obtained from photothermal deflection measurements of optical absorption performed at 1064 nm ($T_a = 0^\circ\text{C}$ denotes as-deposited coatings).

TABLE IV. Annealing treatments applied to sample A.

Run	1	2	3	4	5	6	7
T_a (°C)	120	200	285	330	373	462	550
Δt_a (h)	10	10	10	10	10	10	10

absorption is the cause of the observed degradation of the signal-to-noise ratio. The absorption could be related to the formation of color centers, to the presence of

roughness, or to a poorly stoichiometric structure, where some aluminium particles might not be fully fluorinated [22]. We then use a pole in the UV region and a Tauc-Lorentz oscillator for the optical model of the thin-film layer, which simultaneously fitted all the measured spectra with the same accuracy. A Bruggeman effective-medium approximation surface layer is added to the model to account for possible surface effects such as roughness.

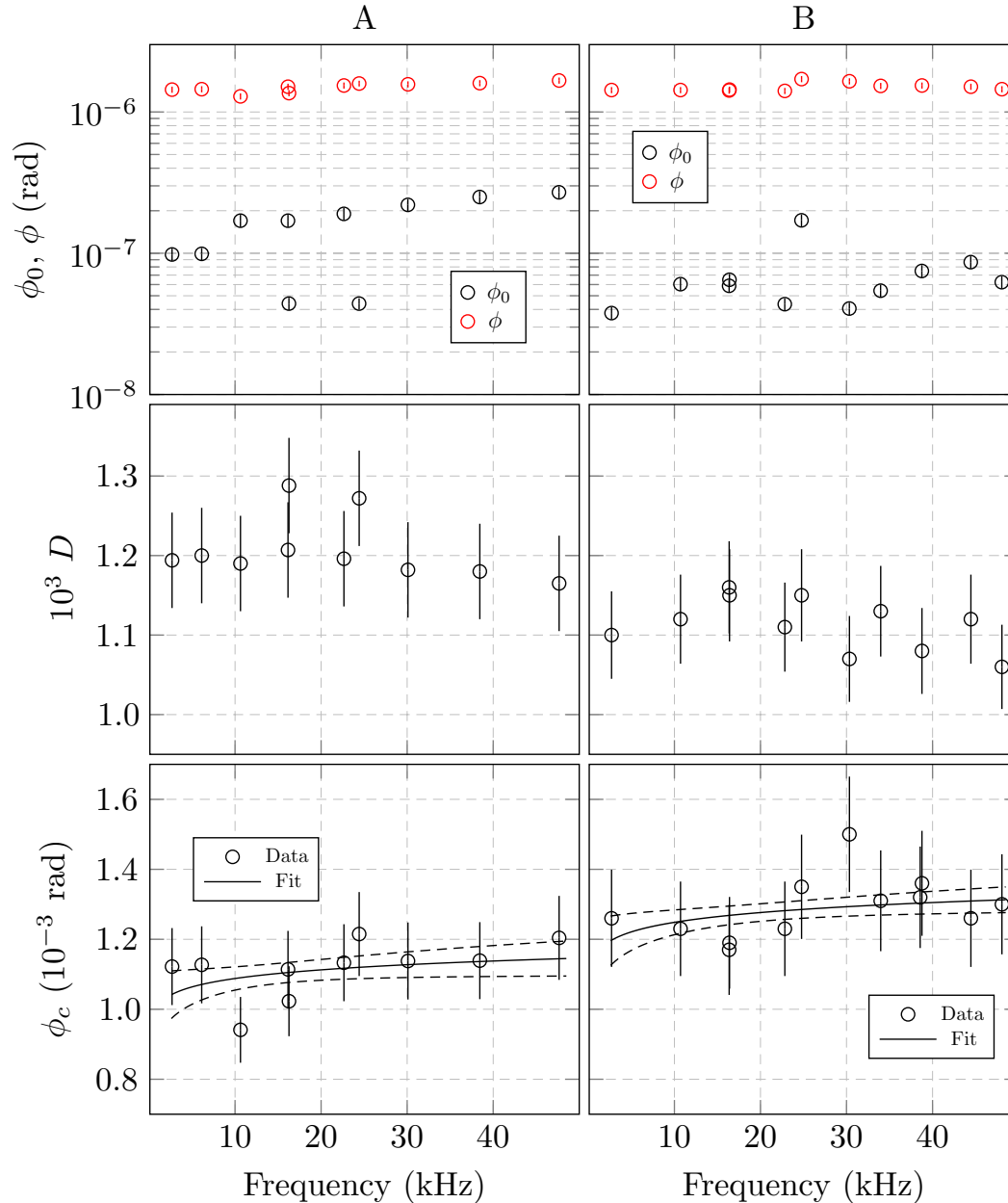


FIG. 7. Characterization of mechanical losses of disks A (left column) and B (right column), as a function of frequency. Top row: measured losses of the disks before (ϕ_0) and after coating (ϕ). Middle row: frequency-dependent dilution factor D . Bottom row: coating loss angle ϕ_c of as-deposited IBS AlF_3 thin films; the best-fit power-law model of Eq. (4) and its confidence interval to one standard deviation are shown with solid and dashed lines, respectively. Coating loss angle values measured on the two disks are compatible within the error bars.

TABLE V. Measured Young's modulus Y , Poisson ratio ν , and best-fit parameters of the power-law model of Eq. (4).

	Y (GPa)	ν	a (10^{-3} rad)	b
Disk A	78 ± 2	0.27 ± 0.02	1.09 ± 0.03	0.03 ± 0.03
Disk B	72 ± 1	0.22 ± 0.03	1.25 ± 0.04	0.03 ± 0.03

Figure 5 shows the dispersion law and the extinction curve derived from our analysis of the as-deposited coatings, and Table III lists our results (including density) against those we found in the literature concerning IBS AlF_3 thin films [20–22]. The Bruggeman layer is found to be almost 4% of the total coating thickness, indicating that the surface condition may play a role in optical loss at low wavelength. Values at $E = 1.17$ eV and $E = 0.80$ eV are particularly relevant, since those photon energies correspond to 1064 and 1550 nm, respectively, which are the operational laser wavelengths of current and future GWDs [7–9,15]. Refractive-index values are $n = 1.358 \pm 0.005$ at 1064 nm and $n = 1.356 \pm 0.005$ at 1550 nm. For comparison, the refractive index at 1064 nm of the IBS silica coatings of present GWDs is $n = 1.47 \pm 0.01$ before annealing [6].

Figure 6 shows the extinction coefficient k obtained from the photothermal deflection measurements of optical absorption at 1064 nm, as a function of the annealing temperature T_a using the measured thickness of 211 nm, as reported in Table I. We assume that loss by light scatter

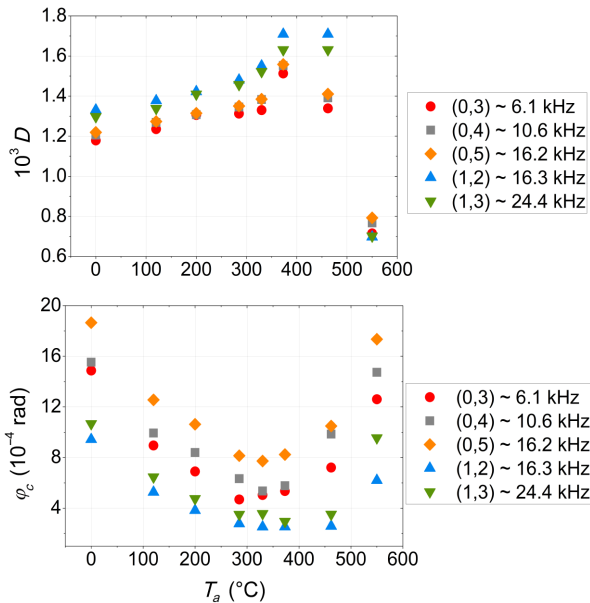


FIG. 8. Sample A: evolution of the dilution factor (top) and coating loss angle (bottom) with annealing temperature for some resonant modes. Errors in dilution factor measurements are approximately 5% and approximately 8% in loss angle measurements.

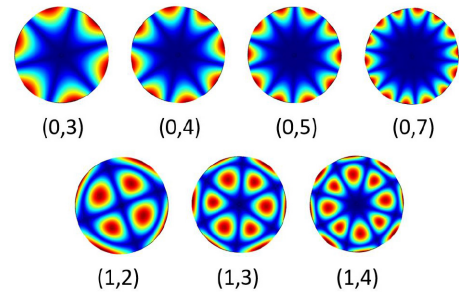


FIG. 9. Resonant modes identified with the (r, a) notation. The color scale represents the amplitude of oscillations from blue (no movement) to red (wider movement). Using a GeNS system it is possible to observe resonant modes with a nodal point in the center.

is negligible. We measure $k = 5.1 \times 10^{-5}$ before treatment, then k increases after each annealing step up to $k = 1.4 \times 10^{-3}$ for $T_a = 300^\circ\text{C}$.

C. Mechanical properties

It is known that postdeposition annealing treatment can improve mechanical properties of a material [6], but it is important to establish both the ideal peak temperature T_a and the duration Δt_a at that temperature.

1. Sample A

Disk A underwent a series of annealing treatments of equal duration Δt_a but of increasing plateau temperature T_a (Table IV). Heating and cooling ramps of 100°C every hour are used.

After each annealing we measure the loss angle φ of the coated silica disk and applying Eqs. (2) and (3) we measure the frequency-dependent dilution factor and extract the coating loss angle φ_c . The results achieved at LMA

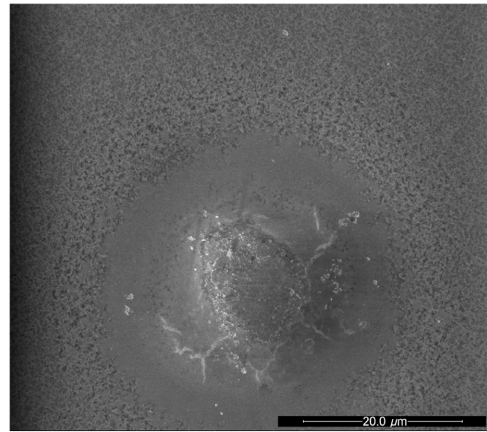


FIG. 10. Sample A: defect formation on the coating surface after the annealing at 330°C . Environmental scanning electron microscope: FEI quanta 200 FEG. Magnification: 5000x.

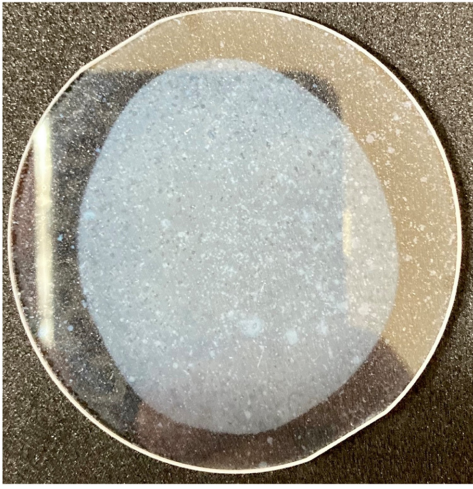


FIG. 11. Sample A: coating surface in contact with the quartz box after the annealing at 550 °C.

before the first annealing treatment are shown in Fig. 7. It is possible to describe the frequency-dependent behavior of the coating loss angle fitting a power-law model to our data via least-squares linear regression [36–38]:

$$\varphi_c(f) = a \left(\frac{f}{10 \text{ kHz}} \right)^b. \quad (4)$$

In Table V are reported the mechanical properties of as-deposited IBS AlF_3 estimated using the procedure described in Sec. IID and the best-fit parameters (a,b) for each sample.

In Fig. 8 are reported the evolutions of dilution factor and coating loss angle with annealing temperature,

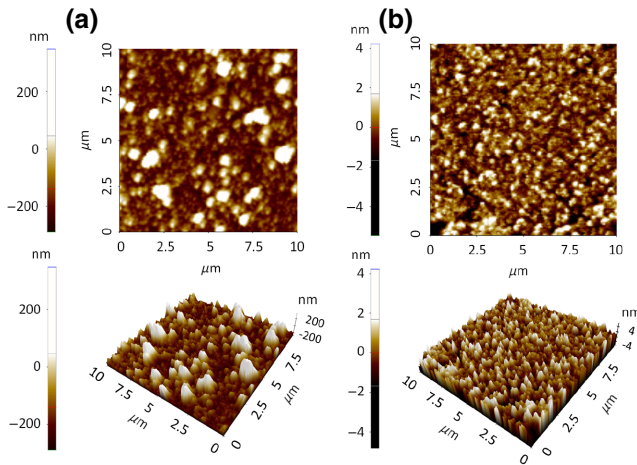


FIG. 12. Morphology of the two sides of sample A measured with AFM (XE100 Park System Inc): side (a) is in contact with the quartz box during the annealing at 550 °C and has a mean roughness of 67.21 nm; side (b) has a mean roughness of 0.614 nm.

TABLE VI. Chemical composition of sample A measured with the spectrometer after the annealing at 550 °C.

Element	Atomic % side (a)	Atomic % side (b)
O	55.3 ± 0.6	52.6 ± 0.6
F	4.4 ± 0.2	7.5 ± 0.4
Al	24.8 ± 0.6	30.8 ± 0.5
Si	15.5 ± 0.9	9.1 ± 0.7

measured at the UniUrb laboratory. The first set of data ($T_a = 0$ °C) represents the measured values before the first annealing. The (r, a) notation denote different vibrational modes with r radial and a azimuthal nodes that are summarized in Fig. 9.

From Fig. 8 it is possible to see that the dilution factor increases until the treatment at 373 °C and that the coating loss angle decreases after each annealing until the treatment at 373 °C. The annealing temperature that minimizes the coating loss angle is between 285 °C and 373 °C.

The mass of the sample remains unchanged until the treatment at 373 °C and a decrease of 0.3 mg is recorded after the annealing at 462 °C and a decrease of 0.4 mg is recorded after the last annealing at 550 °C. So, after the last treatment, we lose 0.7 mg of coating out of 1.8 mg.

Moreover, using the optical microscope, we start to observe some round structures on the surface of the coating after the treatment at 330 °C. An example, recorded using an environmental scanning electron microscope, is reported in Fig. 10.

After the treatment at 550 °C the appearance of the coating changed: the side in contact with the quartz box used inside the furnace during the annealing looked opaque in the center, as shown in Fig. 11. The morphology of the coating, measured with an atomic force microscope (AFM), appears very different on the two sides of the sample: the roughness of the side in contact with the quartz box reported in Fig. 12(a) completely changed from its original value.

Moreover, we observe the surface and the chemical composition of the sample with an environmental scanning electron microscope (FEI quanta 200 FEG equipped with a spectrometer). In Fig. 13 it is possible to observe the formation of crystals on both sides of the sample. Crystals on side (a) are coarser than on side (b). In Table VI we report the chemical compositions of the two sides measured with the spectrometer. The stoichiometry of AlF_3 is not respected: there is a deficiency of fluoride on both sides of the sample. The presence of silicon and oxygen is due to the silica substrate under the coating. It seems that the fluoride reacted with the silicon contained in the quartz box during the thermal treatment at 550 °C producing a volatile compound (SiF_4): this can explain the mass loss, the defects formation on the surface, and the deficiency of fluoride.

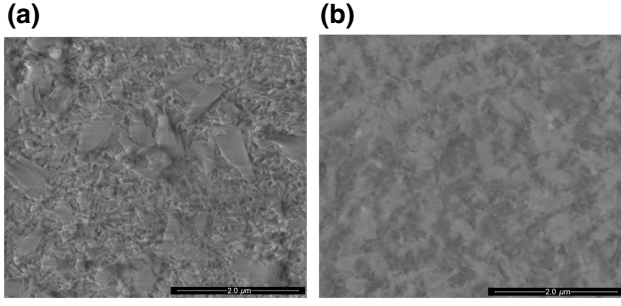


FIG. 13. Crystals formation observed on the two sides of sample A using the environmental scanning electron microscope (FEI quanta 200 FEG equipped with a spectrometer) Magnification: 60000x. Side (a) is in contact with the quartz box during the annealing at 550 °C.

2. Sample B

Disk B, nominally identical to disk A, underwent a series of annealing treatments of equal T_a but of increasing Δt_a (Table VII). We indicate as “cumulative duration” the total amount of time at the plateau temperature.

From the results on sample A, we chose 285 °C as the best annealing temperature, because it minimizes the coating loss angle and seems not to produce defects on its surface. After each annealing we measure the coated disk and applying Eqs. (2) and (3) we measure the frequency-dependent dilution factor and extract the coating loss angle φ_c . The results are reported in Fig. 14. The first set of data ($\Delta t_a = 0$ °C) represents the measured values (at Uni-Urb laboratory) before the first annealing. The coating loss angle decreased after the first treatment, but no more improvements are observed after subsequent annealings.

The mass of the sample remains unchanged after all thermal treatments. No defects or crystals are observed using the optical microscope and the environmental scanning electron microscope.

In Table VIII we report the chemical compositions of the two sides measured with the spectrometer. In this case, there is more fluoride than aluminium; however, the stoichiometry is not respected.

IV. CONCLUSIONS

In the framework of a research activity devoted to find low-noise coating materials for present and future gravitational-wave detectors, we characterize the optical and mechanical properties of a set of IBS AIF₃ thin films.

TABLE VII. Annealing treatments applied to sample B.

Run	1	2	3
T_a (°C)	285	285	285
Δt_a (h)	10	20	30
Cumulative duration (h)	10	30	60

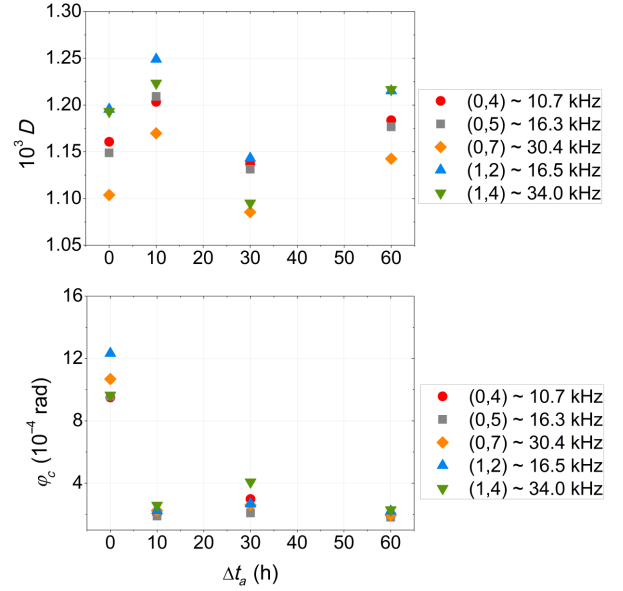


FIG. 14. Sample B: evolution of the dilution factor (top) and coating loss angle (bottom) with annealing time for some resonant modes. Errors in dilution factor measurements are approximately 5% and approximately 8% in loss angle measurements.

We chose fluoride coatings because of their low-refractive index n_L , with the aim of minimizing the overall high-reflection coating thickness t_c in Eq. (1). As a reminder, t_c is a monotonically decreasing function of the refractive-index contrast $C = n_H/n_L$. Furthermore, because of their potentially low mechanical loss at low temperature [23], fluorides could be a valid option for use in cryogenic detectors.

Indeed, the IBS AIF₃ thin films feature a lower refractive index at 1064 nm than that of IBS silica layers of current detectors [6]. However, their optical absorption and ambient-temperature loss angle turned out to be considerably higher.

Concerning the coating loss angle, the best annealing temperature is found to be 285 °C (from the analysis of *sample A*) and a duration of 10 h at the plateau temperature is sufficient to reach a minimum in the coating loss angle $\varphi_c \simeq 2.2 \times 10^{-4}$ rad achieved in sample B. Higher annealing temperatures could produce a chemical reaction between the fluoride of the coating and the silicon contained in the substrate, producing defects on the sample

TABLE VIII. Chemical composition of sample B measured with the spectrometer after the last annealing at 285 °C.

Element	Atomic % side (a)	Atomic % side (b)
O	19.1 ± 0.4	15.2 ± 0.5
F	50.8 ± 0.4	56.1 ± 0.5
Al	28.7 ± 0.3	27.5 ± 0.4
Si	1.4 ± 0.3	1.2 ± 0.2

surface. However, the loss angle of AlF_3 coatings at room temperature is still too high compared with silica coatings, whose value is $\varphi_c \simeq 2.3 \times 10^{-5}$ rad [6]. Further tests will be carried out in the near future to explore the mechanical behavior of AlF_3 coatings at low temperatures, where the silica loss angle increases and should be replaced by another low-refractive-index material.

From a point of view of optical properties, the optical absorption increases after each annealing and is at least 3 orders of magnitude higher than what is tolerable for GWDs applications [6]. In the future, efforts will be made to optimize the quality of the coating material in order to decrease the coating optical absorption and loss angle. Lower optical and mechanical losses could possibly be achieved by changing the coating growth conditions [6], as well as by improving the stoichiometry and reducing the amount of impurities.

ACKNOWLEDGMENTS

This work is promoted by the Laboratoire des Matériaux Avancés and partially supported by the Virgo Coating Research and Development (VCR&D) Collaboration. The authors would like to thank M. Gauch, F. Carstens, and H. Ehlers of the Laser Zentrum Hannover for the production of the AlF_3 thin films and for the fruitful discussions. In the online document repositories of the LIGO and the Virgo Scientific Collaborations, this work is assigned document numbers LIGO-P2100478 and VIR-1385B-21, respectively.

-
- [1] R. X. Adhikari, Gravitational radiation detection with laser interferometry, *Rev. Mod. Phys.* **86.1**, 121 (2014).
- [2] P. R. Saulson, Thermal noise in mechanical experiments, *Phys. Rev. D* **42.8**, 2437 (1990).
- [3] Y. Levin, Internal thermal noise in the LIGO test masses: A direct approach, *Phys. Rev. D* **57.2**, 65.9 (1998).
- [4] H. B. Callen and R. F. Greene, On a theorem of irreversible thermodynamics, *Phys. Rev.* **86.5**, 702 (1952).
- [5] G. M. Harry, A. M. Gretarsson, P. R. Saulson, S. E. Kittelberger, S. D. Penn, W. J. Startin, S. Rowan, M. M. Fejer, D. R. Crooks, G. Cagnoli, and J. Hough, Thermal noise in interferometric gravitational wave detectors due to dielectric optical coatings, *Class. Quantum Gravity* **19.5**, 897 (2002).
- [6] M. Granata, A. Amato, L. Balzarini, M. Canepa, J. Degallaix, D. Forest, V. Dolique, L. Mereni, C. Michel, L. Pinard, and B. Sassolas, Amorphous optical coatings of present gravitational-wave interferometers, *Class. Quantum Gravity* **37.9**, 095004 (2020).
- [7] J. Aasi, B. P. Abbott, and R. Abbott, Classical Quantum Gravity, 32. LIGO Scientific Collaboration 074001 (2002).
- [8] F. Acernese, M. Agathos, K. Agatsuma, D. Aisa, N. Allemandou, A. Allocca, J. Amarni, P. Astone, G. Balestri, G. Ballardin, and F. Barone, Advanced Virgo: a second-generation interferometric gravitational wave detector, *Class. Quantum Gravity* **32.2**, 024001 (2014).
- [9] Y. Aso, Y. Michimura, K. Somiya, M. Ando, O. Miyakawa, T. Sekiguchi, D. Tatsumi, and H. Yamamoto, (The KAGRA Collaboration), Interferometer design of the KAGRA gravitational wave detector, *Phys. Rev. D* **88.4**, 043007 (2013).
- [10] A. E. Villar, E. D. Black, R. DeSalvo, K. G. Libbrecht, C. Michel, N. Morgado, L. Pinard, I. M. Pinto, V. Pierro, V. Galdi, M. Principe, and I. Taurasi, Measurement of thermal noise in multilayer coatings with optimized layer thickness, *Phys. Rev. D* **81.12**, 122001 (2010).
- [11] J. Degallaix, C. Michel, B. Sassolas, A. Allocca, G. Cagnoli, L. Balzarini, V. Dolique, R. Flaminio, D. Forest, M. Granata, and B. Lagrange, Large and extremely low loss: the unique challenges of gravitational wave mirrors, *JOSA A* **36.11**, C85 (2019).
- [12] L. Pinard, C. Michel, B. Sassolas, L. Balzarini, J. Degallaix, V. Dolique, R. Flaminio, D. Forest, M. Granata, B. Lagrange, and N. Straniero, Mirrors used in the LIGO interferometers for first detection of gravitational waves, *Appl. Opt.* **56.4**, C11 (2017).
- [13] M. Granata, A. Amato, G. Cagnoli, M. Coulon, J. Degallaix, D. Forest, L. Mereni, C. Michel, L. Pinard, B. Sassolas, and J. Teillon, Progress in the measurement and reduction of thermal noise in optical coatings for gravitational-wave detectors, *Appl. Opt.* **59.5**, A229 (2020).
- [14] G. Vajente, L. Yang, A. Davenport, M. Fazio, A. Ananyeva, L. Zhang, G. Billingsley, K. Prasai, A. Markosyan, R. Bassiri, and M. M. Fejer, Low Mechanical Loss TiO_2 : GeO_2 Coatings for Reduced Thermal Noise in Gravitational Wave Interferometers, *Phys. Rev. Lett.* **127.7**, 071101 (2021).
- [15] M. Abernathy, F. Acernese, P. Ajith, B. Allen, P. Amaro Seoane, N. Andersson, S. Aoudia, P. Astone, B. Krishnan, L. Barack, and F. Barone, Einstein gravitational wave Telescope conceptual design study. (2011).
- [16] B. P. Abbott, R. Abbott, T. D. Abbott, M. R. Abernathy, K. Ackley, C. Adams, P. Addesso, R. X. Adhikari, V. B. Adya, C. Affeldt, and N. Aggarwal, Exploring the sensitivity of next generation gravitational wave detectors, *Class. Quantum Gravity* **34.4**, 044001 (2017).
- [17] I. W. Martin, R. Nawrodt, K. Craig, C. Schwarz, R. Bassiri, G. Harry, J. Hough, S. Penn, S. Reid, R. Robie, and S. Rowan, Low temperature mechanical dissipation of an ion-beam sputtered silica film, *Class. Quantum Gravity* **31.3**, 035019 (2014).
- [18] M. Granata, L. Balzarini, J. Degallaix, V. Dolique, R. Flaminio, D. Forest, D. Hofman, C. Michel, R. Pedurand, L. Pinard, and B. Sassolas, Internal friction and Young's modulus measurements on SiO_2 and Ta_2O_5 films done with an ultra-high Q silicon-wafer suspension, *Arch. Metall. Mater.* **60**, 365 (2015).
- [19] J. Kolbe, H. Kessler, T. Hofmann, F. Meyer, H. Schink, and D. Ristau, Optical properties and damage thresholds of dielectric UV/VUV coatings deposited by conventional evaporation, IAD, and IBS. Laser-Induced Damage in Optical Materials: 1991. Vol. 1624. SPIE, 1992.
- [20] J. Kolbe and H. Schink, Optical losses of dielectric VUV-mirrors deposited by conventional evaporation, IAD, and IBS. Thin Films for Optical Systems. Vol. 1782. SPIE, 1993.

- [21] T. Yoshida, K. Nishimoto, K. Sekine, and K. Etoh, Fluoride antireflection coatings for deep ultraviolet optics deposited by ion-beam sputtering, *Appl. Opt.* **45.7**, 1375 (2006).
- [22] A. Ode, Ion beam sputtering of fluoride thin films for 193 nm applications, *Appl. Opt.* **53.4**, A330 (2014).
- [23] C. Schwarz, D. Heinert, P. Seidel, A. Tünnermann, G. Hammond, and R. Nawrodt, Mechanical loss of calcium fluoride at cryogenic temperatures, *Phys. Status Solidi (a)* **208.12**, 2719 (2011).
- [24] www.lzh.de.
- [25] H. Fujiwara, *Spectroscopic Ellipsometry: Principles and Applications* (John Wiley & Sons, New York, 2007).
- [26] Alex Amato, S. Terreni, V. Dolique, D. Forest, G. Gemme, M. Granata, L. Mereni, C. Michel, L. Pinard, B. Sassolas, and J. Teillon, Optical properties of high-quality oxide coating materials used in gravitational-wave advanced detectors, *J. Phys.: Mater.* **2.3**, 035004 (2019).
- [27] A. C. Boccara, D. Fournier, W. Jackson, and N. M. Amer, Sensitive photothermal deflection technique for measuring absorption in optically thin media, *Opt. Lett.* **5.9**, 377 (1980).
- [28] A. Nowick and B. Berry, *Anelastic Relaxation in Crystalline Solids* (Academic Press, New York, 1972), 582
- [29] Tianjun Li, F. A. Sandoval, M. Geitner, L. Bellon, G. Cagnoli, J. Degallaix, V. Dolique, R. Flaminio, D. Forest, M. Granata, and C. Michel, Measurements of mechanical thermal noise and energy dissipation in optical dielectric coatings, *Phys. Rev. D* **89.9**, 092004 (2014).
- [30] M. Granata, A. Amato, M. Bischì, M. Bazzan, G. Cagnoli, M. Canepa, M. Chicoine, A. Di Michele, G. Favaro, D. Forest, and G. M. Guidi, Optical and Mechanical Properties of Ion-Beam-Sputtered MgF₂ Thin Films for Gravitational-Wave Interferometers, *Phys. Rev. Appl.* **17.3**, 034058 (2022).
- [31] E. Cesarini, M. Lorenzini, E. Campagna, F. Martelli, F. Piergiovanni, F. Vetrano, G. Losurdo, and G. Cagnoli, A “gentle” nodal suspension for measurements of the acoustic attenuation in materials, *Rev. Sci. Instrum.* **80.5**, 053904 (2009).
- [32] G. Vajente, A. Ananyeva, G. Billingsley, E. Gustafson, A. Heptonstall, E. Sanchez, and C. Torrie, A high throughput instrument to measure mechanical losses in thin film coatings, *Rev. Sci. Instrum.* **88.7**, 073901 (2017).
- [33] M. Granata, E. Saracco, N. Morgado, A. Cajgfinger, G. Cagnoli, J. Degallaix, V. Dolique, D. Forest, J. Franc, C. Michel, and L. Pinard, Mechanical loss in state-of-the-art amorphous optical coatings, *Phys. Rev. D* **93.1**, 012007 (2016).
- [34] J. F. Ziegler, Nuclear Instruments and Methods in Physics Research Section B: Beam Interactions with Materials and Atoms Volumes 219–220, 2004, p. 1027-1036, ISSN 0168-583X, .
- [35] P. Villars and K. Cenzual, AIF₃ Crystal Structure: Datasheet from PAULING FILE Multinaries Edition 2012, SpringerMaterials.
- [36] K. S. Gilroy and W. A. Phillips, An asymmetric double-well potential model for structural relaxation processes in amorphous materials, *Philos. Mag. B* **435**, 73.5 (1981).
- [37] F. Travasso, P. Amico, L. Bosi, F. Cottone, A. Dari, L. Gammaitoni, H. Vocca, and F. Marchesoni, Low-frequency internal friction in silica glass, *EPL (Europhys. Lett.)* **80.5**, 50008 (2007).
- [38] G. Cagnoli, M. Lorenzini, E. Cesarini, F. Piergiovanni, M. Granata, D. Heinert, F. Martelli, R. Nawrodt, A. Amato, Q. Cassar, and J. Dickmann, Mode-dependent mechanical losses in disc resonators, *Phys. Lett. A* **382.33**, 2165 (2018).